



# Replication of SMSI via ALD: TiO<sub>2</sub> Overcoats Increase Pt-Catalyzed Acrolein Hydrogenation Selectivity

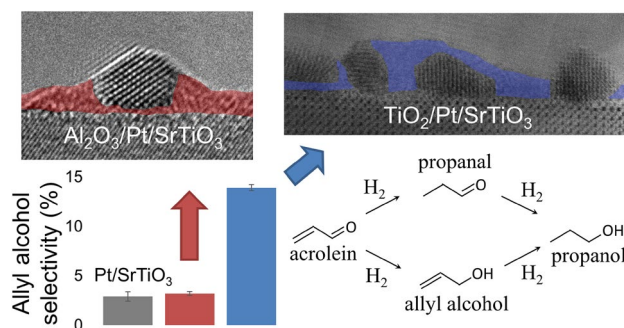
Robert M. Kennedy<sup>1</sup> · Lawrence A. Crosby<sup>2</sup> · Kunlun Ding<sup>3</sup> · Christian P. Canlas<sup>4</sup> · Ahmet Gulec<sup>2</sup> · Laurence D. Marks<sup>2</sup> · Jeffrey W. Elam<sup>4</sup> · Christopher L. Marshall<sup>5</sup> · Kenneth R. Poeppelmeier<sup>1,5</sup> · Peter C. Stair<sup>1,5</sup>

Received: 26 April 2018 / Accepted: 8 June 2018  
© Springer Science+Business Media, LLC, part of Springer Nature 2018

## Abstract

The effects of sub-nanometer atomic layer deposition films of titania and alumina are compared for the acrolein hydrogenation selectivity of Pt/SrTiO<sub>3</sub> catalysts. The titania-overcoated catalyst is similar to strong metal-support interaction catalysts formed by high temperature reduction, with a thin titania film on top of the supported Pt nanoparticles and an increase in allyl alcohol selectivity, neither of which are observed for the alumina-overcoated catalyst.

## Graphical Abstract



**Keywords** Strong metal support interaction · SMSI · Selective hydrogenation · Acrolein · Platinum · SrTiO<sub>3</sub> · Atomic layer deposition · Nanocrystal support

## 1 Introduction

The strong metal-support interaction (SMSI) is remarkable both for the magnitude of its effect on supported metal catalysts and for the challenges in characterizing and commercializing it. SMSI was discovered by Tauster

et al. when they observed H<sub>2</sub> and CO chemisorption drop to almost zero on Pt/TiO<sub>2</sub> that had been reduced under hydrogen at “high” temperatures (high temperature reduction, HTR) [1]. Further investigation showed that SMSI could be generated for metal particles (M<sub>np</sub>) supported on “reducible” oxides like TiO<sub>2</sub>, which can either become oxygen deficient or form sub-oxides when heated under reducing conditions [1–3]. Early models for SMSI theorized that HTR imbued some electronic effect between the oxide support and the metal nanoparticle, which drastically decreased the binding strength of chemisorbed hydrogen or carbon monoxide [1, 4]. However, as analytical techniques improved, it was discovered that the decrease in chemisorption was primarily a result of the

**Electronic supplementary material** The online version of this article (<https://doi.org/10.1007/s10562-018-2458-5>) contains supplementary material, which is available to authorized users.

✉ Peter C. Stair  
pstair@northwestern.edu

Extended author information available on the last page of the article

metal nanoparticles becoming coated by migrating clusters of the support oxide, thereby blocking access to most of the metal particle surface [5–10]. For many catalytic reactions, SMSI is a potential problem to be avoided—it directly decreases the number of available active sites [6, 11–14]. However, it was discovered that in the case of reactions involving C=O bonds, SMSI could greatly increase activity and selectivity [15–17]. The increased performance of SMSI catalysts for activating carbonyl or nitro groups (carbonyl or nitro hydrogenation, CO oxidation, etc.) is ascribed to stabilization of the group at interfacial sites where the metal particle surface and the overcoat meet [11, 15, 16, 18–25]. The SMSI state can be reversed by re-oxidation, which causes a loss of reduced interfacial sites, migration of the overcoat off of the metal particles, or a combination of both, resulting in a loss of C=O bond selectivity and/or an increase in chemisorption on the metal particles [10, 14, 15, 26–29]. There is a thermodynamic driving force for decoration of the  $M_{np}$  surface by an oxide overcoat when the sum of the surface free energy of the oxide and the metal/oxide interfacial free energy is less than the surface free energy of the metal nanoparticle [10, 30]. For SMSI catalysts, this driving force is increased on reduction of the support (forming the overcoat) and decreased when oxidized (driving the oxide off of the  $M_{np}$  surface). The challenge for commercializing SMSI is in finding new ways to stabilize the activated overcoat on the metal particle. As atomic layer deposition (ALD) creates overcoats that are visibly similar to the SMSI overcoats created by HTR, we sought to determine whether SMSI could be recreated by depositing ALD oxide overcoats on top of a supported metal nanoparticle.

Selective  $\alpha,\beta$ -unsaturated aldehyde hydrogenation is a useful test reaction for SMSI; most noble metal catalysts preferentially hydrogenate olefin groups, while SMSI catalysts using the same noble metal nanoparticles exhibit increased (up to 100%) selectivity for aldehyde hydrogenation [15, 16, 18–20, 22, 31–35]. In addition, the selective hydrogenation of  $\alpha,\beta$ -unsaturated aldehydes to unsaturated alcohols is industrially relevant for biofuels (e.g. furfural), plastics, fine chemicals, and pharmaceuticals [21, 36–39]. Acrolein,  $\text{CH}_2\text{CHCHO}$ , is the simplest molecule to contain a conjugated aldehyde (carbonyl) and olefin group. With acrolein, selectivity differences resulting from the hydrogenation of the two different functional groups can be studied with minimal secondary products or steric effects on selectivity. Acrolein is hydrogenated by addition to either the olefin (propanal), or the aldehyde group (allyl alcohol) [20, 35, 40]. Both products can be hydrogenated a second time to form the fully saturated 1-propanol [41]. The decarbonylation of acrolein to ethylene and carbon monoxide can also occur [33, 42]. While not definitive by

itself, an increase in the aldehyde hydrogenation selectivity of a noble metal catalyst is a strong indication of SMSI.

ALD is a method for self-limiting vapor-phase deposition, in which surface saturation of gas-phase metal precursors on the support controls the rate of deposition [43–46]. The metal precursors alternate with a second gas, which removes the remaining ligands from the metal precursors and regenerates binding groups on the surface. The metal deposition and regeneration steps can be cycled to grow increasingly thick films of metal oxides (or sulfides, nitrides, etc.) or larger metal nanoparticles with controlled size or thickness on low and high surface area materials. Growth by ALD provides increased control over metal nanoparticle size, shape, and distribution compared to conventional wet impregnation methods [47]. ALD oxide overcoats have previously been used to prevent leaching [48], coking [49], and sintering of supported metal catalysts [50, 51].

Platinum nanoparticles on strontium titanate nanocuboids ( $\text{Pt}/\text{SrTiO}_3$ ) are used in this work as model supported platinum catalysts because of the controlled epitaxy of Pt nanoparticles ( $\text{Pt}_{np}$ ) on the (100) facet of the  $\text{SrTiO}_3$  nanocuboids. Model catalysts are designed to have reduced complexity, so that specific effects can be isolated and studied [52].  $\text{SrTiO}_3$  nanocuboids hydrothermally synthesized in an alkaline water/ethanol/acetate solution have primarily (100) facets with a  $\text{TiO}_2$  double-layer surface termination [53–56]. Pt nanoparticles deposited on the  $\text{SrTiO}_3$ -(100) facets have a cube-on-cube epitaxy with a Winterbottom shape that is thermodynamically stable and resistant to sintering [57–60]. We have previously examined the effect of  $\text{Ba}_x\text{Sr}_{1-x}\text{TiO}_3$  nanocuboid supports on the structure sensitivity of Pt for acrolein hydrogenation [34, 35]. Shape control of the Pt nanoparticles by the support simplifies the correlation of the catalytic activity with structural properties [61].

In this study, ALD of titania and alumina on  $\text{Pt}/\text{SrTiO}_3$  is used to mimic the overcoats formed by SMSI in HTR- $\text{Pt}/\text{TiO}_2$  catalysts. Since alumina is not reducible at typical HTR temperatures, the ALD approach provides a methodology to compare reducible and nonreducible overcoats. It is expected, based on the defective structure of as-deposited ALD titania films and analysis of the structure of HTR- $\text{Pt}/\text{TiO}_2$  overcoats, that the ALD titania overcoat will exhibit SMSI behavior and increase aldehyde hydrogenation selectivity versus the undecorated  $\text{Pt}/\text{SrTiO}_3$ , while the ALD alumina overcoat will not [15, 62]. In addition, ALD titania overcoats have been shown to increase the rate of CO oxidation for noble metal catalysts [63–65], another SMSI-sensitive reaction [26]. For SMSI catalysts, the thin oxide overcoat formed during HTR blocks the majority of the  $M_{np}$  sites [10], while creating new sites at the interface of the overcoat and the remaining  $M_{np}$  sites, which preferentially bind C=O [21]. Like HTR, ALD of titania and alumina over  $\text{Pt}/\text{SrTiO}_3$  will form overcoats that cover the  $\text{Pt}_{np}$  (coverage

dependent on overcoat thickness and interfacial energies) [10, 30]. However, defects in the ALD overcoat leading to interfacial site formation and SMSI selectivity is only expected for the reducible titania, and not for the refractory alumina [2]. Here, we seek to demonstrate that the effect of SMSI on hydrogenation selectivity can be generated by ALD of titania overcoats on supported Pt nanoparticles, and compare them to overcoats that cannot be formed by HTR (e.g. alumina) [2, 46].

## 2 Experimental

### 2.1 Catalyst Preparation

The support materials used in this study were SrTiO<sub>3</sub> nanocuboids, synthesized following the previously published procedure by Rabuffetti et al. [66]. The Pt nanoparticles and oxide overcoats were deposited onto the SrTiO<sub>3</sub> nanocuboids by ALD using a viscous flow reactor and adapting methods described previously [59, 67, 68]. The SrTiO<sub>3</sub> nanocuboids were cleaned prior to Pt and alumina ALD in the reactor with 10% O<sub>3</sub> in O<sub>2</sub> for 100 s at 300 °C. The Pt ALD used alternating 120 s exposures of (methylcyclopentadienyl) trimethylplatinum (MeCpPtMe<sub>3</sub>) and 10% O<sub>3</sub> in O<sub>2</sub> at 300 °C, separated by 120 s N<sub>2</sub> purges. The TiO<sub>2</sub> ALD used titanium tetraisopropoxide (TTIP) and deionized H<sub>2</sub>O at 200 °C, and the Al<sub>2</sub>O<sub>3</sub> ALD used trimethyl aluminum (TMA) and deionized H<sub>2</sub>O at 200 °C. First, 5 Pt ALD cycles were performed on 1.00 g of the SrTiO<sub>3</sub> nanocuboid powder (Pt/SrTiO<sub>3</sub>) [59]. From this sample, about 0.20 g was overcoated with 5 cycles of Al<sub>2</sub>O<sub>3</sub> ALD (Al<sub>2</sub>O<sub>3</sub>/Pt/SrTiO<sub>3</sub>), and an additional 0.20 g was overcoated with 10 cycles of TiO<sub>2</sub> ALD (TiO<sub>2</sub>/Pt/SrTiO<sub>3</sub>) [49, 69].

### 2.2 Catalyst Characterization

The catalyst loading was determined by inductively coupled plasma optical emission spectroscopy (ICP-OES), using a Thermo iCAP 7600 ICP-OES. Four samples were measured: SrTiO<sub>3</sub>, Pt/SrTiO<sub>3</sub>, Al<sub>2</sub>O<sub>3</sub>/Pt/SrTiO<sub>3</sub>, and TiO<sub>2</sub>/Pt/SrTiO<sub>3</sub>. The surface loadings of Pt, Al<sub>2</sub>O<sub>3</sub>, and TiO<sub>2</sub> on the SrTiO<sub>3</sub> nanocuboids were calculated via the ICP concentrations. The catalyst surface areas were measured on a Micrometrics 3Flex, using the Brunauer–Emmett–Teller (BET) theory for gas adsorption [70]. Samples were degassed in N<sub>2</sub> at 300 °C for 1 h prior to BET measurements. N<sub>2</sub> adsorption isotherms were measured at –196 °C. The accessible specific Pt surface area (S<sub>Pt</sub>) was determined by carbon monoxide chemisorption using an Altamira Instruments AMI-200 as moles of surface Pt atoms (Pt<sub>surf</sub>) per gram of catalyst (mol Pt<sub>surf</sub>/g cat.), assuming that each accessible Pt<sub>surf</sub> linearly adsorbed one CO molecule [71]. The BET and CO chemisorption

measurements were performed in the CleanCat user facility at NU. Additional details of ICP and CO chemisorption preparation and analysis are reported in the Electronic Supplementary Materials.

The size and distribution of Pt<sub>np</sub> in the Pt/SrTiO<sub>3</sub> sample was examined using a Hitachi HD-2300A Dual EDS scanning transmission electron microscope (STEM). The Al<sub>2</sub>O<sub>3</sub>/Pt/SrTiO<sub>3</sub> and TiO<sub>2</sub>/Pt/SrTiO<sub>3</sub> samples were characterized by high resolution electron microscopy (HREM), using a JEOL 2100F as well as a probe-corrected JEOL JEM-ARM200CF. Energy dispersive X-ray spectroscopy (EDS) line scans were acquired in combination with annular bright field (ABF) and high angle annular dark field (HAADF) images using the ARM200CF operating at 200 kV accelerating voltage. The collection angles for the ABF images were 17–45 mrad and were 68–280 mrad for the HAADF. The EDS line scans were collected with the SrTiO<sub>3</sub> nanocuboids oriented in the [001] direction with respect to the electron beam. The line scan was aligned to be perpendicular to a (100) facet of SrTiO<sub>3</sub>, and centered on a Pt nanoparticle. The line scan extended from the support out into the vacuum above the Pt nanoparticle. EDS data were collected for the O-, Ti-, Sr-, and Al-K peaks, and the Pt-L peaks.

### 2.3 Catalytic Testing for Selective Hydrogenation

Vapor-phase hydrogenation of acrolein was run in a plug-flow reactor with a GC-FID/TCD (Figure S1). Research-grade argon and hydrogen (Airgas) were used; the gas composition was controlled by varying the relative feed rates of H<sub>2</sub> and Ar via 100 sccm mass flow controllers. Lines were heated with electric heat tapes to 100 °C to minimize condensation of acrolein or products. Acrolein (90% v/v in water with hydroquinone stabilizer, Sigma Aldrich) was pumped as a liquid into the heated lines using a VICI M6 syringe-free pump. Acrolein is a lachrymator and highly toxic; additional information on its handling and the liquid pump can be found in the Electronic Supplementary Materials. Pressure gauges and pressure relief valves were located before and after the reactor to detect and prevent overpressurization caused by plugging. The catalyst bed was in a ¼" O.D. stainless steel reactor in a vertical tube furnace, and the temperature was monitored via a K-type thermocouple located in the catalyst bed. Conversion from the reactor tube and thermocouple was negligible. Quartz wool was used to support the catalyst. The catalyst sample (5–50 mg) was diluted with α-alumina (300 mg, Alundum Norton "RR" 60 mesh α-alumina, Fisher Scientific). Sample loads for each run are listed in Table S2. Catalytic tests were performed at 100 °C, and reduction pre-treatments were at 200 °C. Additional details of the reactor design and the pretreatment method can be found in the Electronic Supplementary Materials.

Gas analysis was done on an Agilent 6890 series GC with both a thermal conductivity detector (TCD) and a flame ionization detector (FID). Data was collected at 8 min intervals, constrained by the residence time of allyl alcohol in the GC column. Two columns were used in conjunction with the TCD to separate the light gases ( $H_2$ ,  $N_2$ ,  $O_2$ ,  $CO$ ,  $CO_2$ ,  $CH_4$ ): a 30 m  $\times$  0.53 mm ResTek TR-QPlot for  $CO_2$  and a 30 m  $\times$  0.53 mm ResTek RT-MolSieve 5A for all other gases. The FID was used for detecting the organic feed and products using a 30 m  $\times$  0.32 mm Alltech EC-wax column, with 0.25  $\mu$ m film thickness. The GC oven was held constant at 50  $^\circ$ C and the gas sampling valve box was held at 125  $^\circ$ C.

### 3 Results and Discussion

#### 3.1 Atomic Layer Deposition

Strontium titanate nanocuboids (BET surface area 19  $m^2/g$ ) were used as a support for Pt nanoparticles grown by ALD (21  $m^2/g$ ), which were then overcoated with either alumina (18  $m^2/g$ ) or titania (21  $m^2/g$ ) by ALD (Table 1). The average Pt weight loading was determined by ICP-OES to be 4, 3, and 3 wt% Pt for Pt/SrTiO<sub>3</sub>, Al<sub>2</sub>O<sub>3</sub>/Pt/SrTiO<sub>3</sub>, and TiO<sub>2</sub>/Pt/SrTiO<sub>3</sub>, respectively (Table S1). The Al<sub>2</sub>O<sub>3</sub>/Pt/SrTiO<sub>3</sub> sample had an alumina overcoat loading of 5 wt%, calculated from the Al loading of 2.7 wt%. For TiO<sub>2</sub>/Pt/SrTiO<sub>3</sub>, the mass gain from titania ALD was 4 wt% and the mol/mol Ti:Pt ratio calculated from ICP was elevated from a near-stoichiometric 1.02:1 ( $\pm$ 0.02) for Pt/SrTiO<sub>3</sub> to 1.10:1 (Table S1). After ALD oxide overcoating, 5 cycles of alumina ALD had covered 34% of Pt<sub>surf</sub>, while 10 cycles of titania ALD had covered 95.7% of Pt<sub>surf</sub> (Table 1). Optical microscopy, TEM images, analysis of Pt ALD, and the calculations for the average overcoat thickness can be found in the Electronic Supplementary Materials.

#### 3.2 Overcoat Morphology

HREM (Fig. 1) and combined BF/HAADF/EDS (Fig. 2) were used to examine the overcoat morphology at the

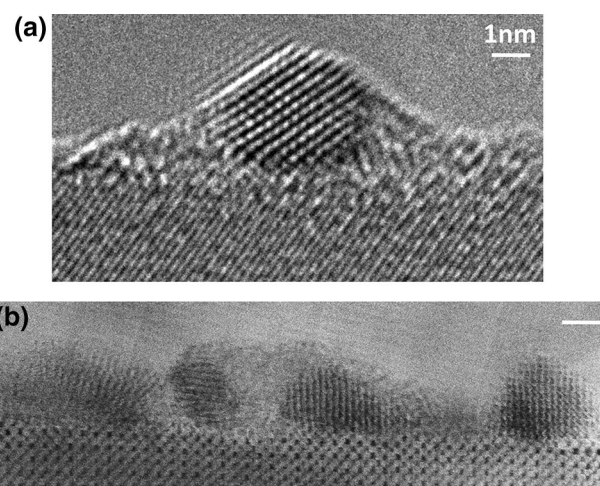


**Fig. 1** HREM micrographs of ALD overcoats of alumina (a) and titania (b) on Pt/SrTiO<sub>3</sub>. The ALD overcoats are visible as an amorphous film a at the perimeter of the Pt<sub>np</sub> and b over the top of the Pt<sub>np</sub>, as well as on the surface of SrTiO<sub>3</sub> for both catalysts

Pt/SrTiO<sub>3</sub> surface. The BF/HAADF/EDS samples were imaged along the [001] axis of SrTiO<sub>3</sub>, showing Pt<sub>np</sub> on the (100) facet of SrTiO<sub>3</sub>. EDS was collected in a line scan, indicated as a purple line in the BF and HAADF micrographs. The alumina and titania overcoats are both visible as approximately one nanometer-thick amorphous oxide films on the surface of Pt/SrTiO<sub>3</sub> (Fig. 1) [72]. However, alumina is localized on the SrTiO<sub>3</sub> surface (Figs. 1a, 2a), while titania is present on top of both the SrTiO<sub>3</sub> support and the Pt<sub>np</sub> (Figs. 1b, 2d). As the alumina and titania overcoats are amorphous, they have low contrast in HAADF and are not apparent in Fig. 2b, e [73]. The peak maximum of the Al EDS signal above the SrTiO<sub>3</sub> surface (Fig. 2c) corresponds to the approximately one nanometer-thick alumina film observed in the micrographs (Fig. 1a). The TiO<sub>2</sub> overcoat could not be differentiated from the SrTiO<sub>3</sub> support by Ti EDS (Fig. 2f, see the Electronic Supplementary Materials for more information). The approximately 1 nm titania ALD film on Pt/SrTiO<sub>3</sub> (Table 1; Figs. 1b, 2d) is visibly similar to the overcoat formed on HTR SMSI

**Table 1** BET surface area, CO chemisorption, and conversion per gram normalized to Pt/SrTiO<sub>3</sub>

Sample	Surface area (m <sup>2</sup> /g)	S <sub>Pt</sub> (mol Pt <sub>surf</sub> /g cat.)	Pt dispersion (%)	Pt <sub>surf</sub> covered by overcoat (%)	% of Pt/SrTiO <sub>3</sub> conversion <sup>b</sup> (%)
Pt/SrTiO <sub>3</sub>	21(2)	$5.57 \times 10^{-5}$	28.4	—	—
Al <sub>2</sub> O <sub>3</sub> /Pt/SrTiO <sub>3</sub>	18(2)	$3.67 \times 10^{-5}$	16.3	34.0	50
TiO <sub>2</sub> /Pt/SrTiO <sub>3</sub>	21(2)	$2.37 \times 10^{-6}$	1.4	95.7	2
SrTiO <sub>3</sub> <sup>a</sup>	19(2)	—	—	—	—

<sup>a</sup>No platinum present

<sup>b</sup>(% conversion/g overcoat catalyst)/(% conversion/g Pt/SrTiO<sub>3</sub>)

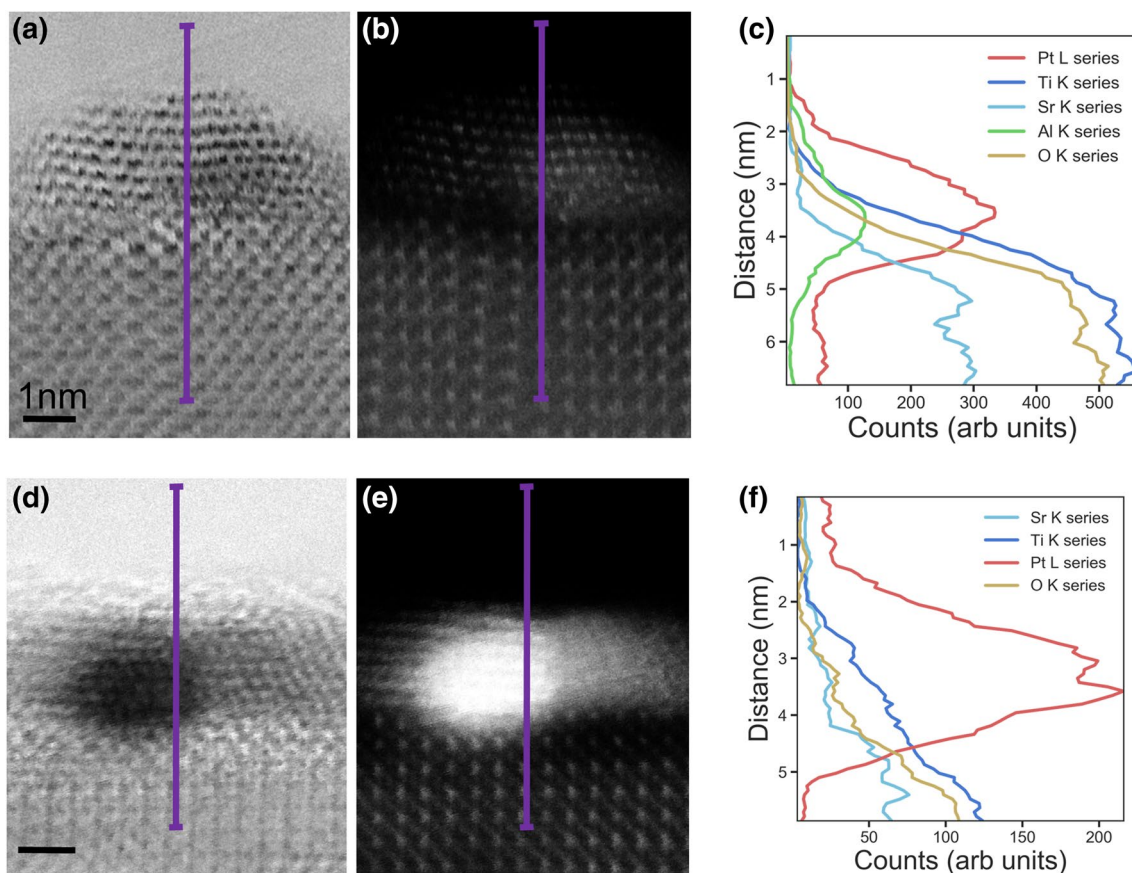


**Fig. 2** Combined BF/HAADF/EDS of Al<sub>2</sub>O<sub>3</sub>/Pt/SrTiO<sub>3</sub> (a–c) and TiO<sub>2</sub>/Pt/SrTiO<sub>3</sub> (d–f). The BF (a, d) and HAADF (b, e) images show Pt<sub>np</sub> on the (100) facet of SrTiO<sub>3</sub> nanocuboids. The EDS line scan path is shown in purple. An amorphous alumina film can be seen at the sides of the Pt<sub>np</sub> in BF (a), and an amorphous titanium oxide film

is visible on the top and sides of the Pt<sub>np</sub> in BF (d). Neither amorphous film has a high contrast in HAADF (b, e). EDS of Al<sub>2</sub>O<sub>3</sub>/Pt/SrTiO<sub>3</sub> (c) indicates that the alumina overcoat (Al K $\alpha$ , green) is concentrated at the SrTiO<sub>3</sub> surface. The titania overcoat could not be distinguished from the Ti in the SrTiO<sub>3</sub> support by EDS (f)

catalysts, appearing on both the Pt<sub>np</sub> and oxide support [9, 10, 12].

The ALD titania film (TiO<sub>2</sub>/Pt/SrTiO<sub>3</sub>) covers 95.7% of Pt<sub>surf</sub>, as measured by CO chemisorption (Table 1), while HTR covers > 90% of Pt<sub>surf</sub> (measured as the difference in chemisorption between samples reduced below and above the HTR temperature of the support) [16]. The ALD alumina film (Al<sub>2</sub>O<sub>3</sub>/Pt/SrTiO<sub>3</sub>), while having approximately the same average thickness, only blocks 34.0% of Pt<sub>surf</sub>. The increased coverage of the Pt<sub>np</sub> on Pt/SrTiO<sub>3</sub> by the titania overcoat can also be seen in the average acrolein conversion: Al<sub>2</sub>O<sub>3</sub>/Pt/SrTiO<sub>3</sub> was 50% as active per gram as Pt/SrTiO<sub>3</sub>, while TiO<sub>2</sub>/Pt/SrTiO<sub>3</sub> had only 2% the activity (Table 1). Conversion was linearly proportional to both the mass of catalyst and Pt<sub>surf</sub>, as would be expected for a pseudo-first order rate, constant gas flow, and low conversions [74]. The proportional decreases in Pt<sub>surf</sub> and conversion from Pt/SrTiO<sub>3</sub> to Al<sub>2</sub>O<sub>3</sub>/Pt/SrTiO<sub>3</sub> to TiO<sub>2</sub>/Pt/SrTiO<sub>3</sub> indicate that the deposition of alumina primarily on SrTiO<sub>3</sub>, and titania on both Pt<sub>np</sub> and SrTiO<sub>3</sub>, as observed in Fig. 1a, b

(respectively), is consistent across the entire sample and not limited to the imaged areas. The difference in coverage of the Pt<sub>np</sub> by the two oxides is notable, as the average film thickness as calculated by weight percent and surface area is approximately the same (alumina: 6 Å, titania: 5 Å, see the Electronic Supplementary Materials for calculations.) The increased deposition of titania on the Pt<sub>np</sub>, similar to the HTR overcoats of SMSI catalysts, may be a result of decreased interfacial energy between titania and Pt (versus alumina and Pt) [10, 30, 75–78].

The turnover frequencies (TOF) of the three catalysts are all within an order of magnitude, ranging from 0.2 to 0.8 s<sup>-1</sup>. The TOF is calculated from the product formation rate (moles of acrolein converted per second), the mass of catalyst, and the number of catalytic sites per mass of catalyst, using Eq. (1). The number of catalytic sites is equal to Pt<sub>surf</sub>, under the assumption that every Pt<sub>surf</sub> measured by CO chemisorption is catalytically active. Pt/SrTiO<sub>3</sub> had the highest average TOF, followed by TiO<sub>2</sub>/Pt/SrTiO<sub>3</sub>, and then Al<sub>2</sub>O<sub>3</sub>/Pt/SrTiO<sub>3</sub> (Table S7, Fig. 3). TOF decreased

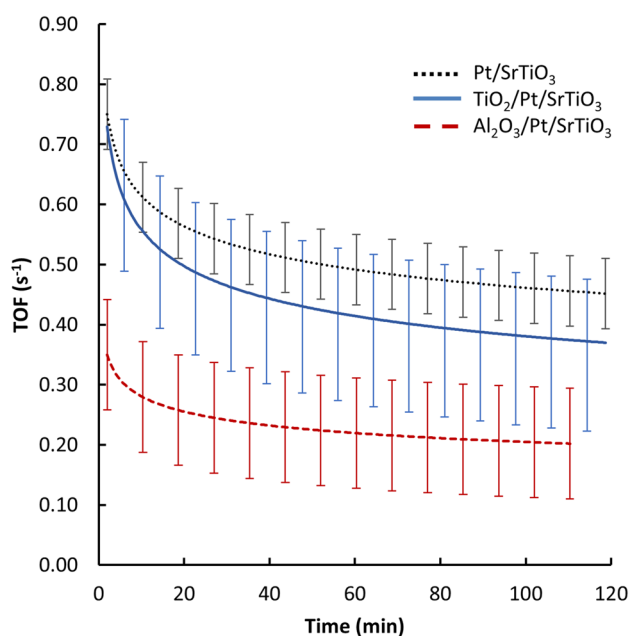


**Fig. 3** Average TOF versus time for  $\text{Al}_2\text{O}_3/\text{Pt}/\text{SrTiO}_3$ ,  $\text{TiO}_2/\text{Pt}/\text{SrTiO}_3$ , and  $\text{Pt}/\text{SrTiO}_3$  (bottom to top). Error bars indicate  $\pm 2\sigma$  of the fit

with time for all three catalysts, as a result of a decrease in conversion, previously ascribed to blocking of Pt sites by strongly adsorbed species [18]. The TOF of HTR catalysts can be orders of magnitude higher for carbonyl hydrogenation than for samples prepared without HTR [16]. The combination of the high activity of the selective SMSI interfacial sites and high number density of SMSI sites in a HTR catalyst result in the increase in TOF after HTR. In a study of the effects of ALD titania overcoating of Pt on the selectivity of crotonaldehyde hydrogenation, it was observed that the overall activity decreased with the number of ALD cycles, while selectivity to alcohols initially increased and then plateaued [62]. If it is assumed that every platinum atom next to the metal oxide interface is selective (and has SMSI activity), the activity and selectivity for alcohols should increase linearly with oxide coverage, corresponding to an increase in the interface perimeter. However, the relatively low activity of the catalysts with ALD titania films (in comparison with HTR films) both here and in [62] suggest that a lower

percentage of the interfacial sites in the ALD overcoats are SMSI active, and that an additional reduction step may be necessary to increase the concentration of SMSI sites at the interface. If the percent of SMSI sites to total catalytic sites is low, the overall TOF will be close to that of the unmodified metal catalyst, but there may be a disproportionate change in selectivity from the small number of highly active and selective SMSI sites, as seen here.

$$\text{Products} \left( \frac{\text{mol}}{\text{s}} \right) \times \frac{1}{\text{cat. (g)}} \times \frac{\text{cat. (g)}}{P_{t, \text{surf}} (\text{mol})} = \text{TOF} (\text{s}^{-1}) \quad (1)$$

The chemisorption, catalytic activity, and TEM data all indicate that sub-nanometer ALD titania film on  $\text{Pt}/\text{SrTiO}_3$  mimics the SMSI morphology of HTR- $\text{Pt}/\text{TiO}_2$ . ALD alumina deposition was different from both ALD titania and SMSI overcoats. ALD alumina was observed only on the oxide support; loss of  $\text{Pt}_{\text{np}}$  surface area was a result of the ALD alumina building up and covering the sides of the  $\text{Pt}_{\text{np}}$ , rather than from alumina forming directly on top of the  $\text{Pt}_{\text{np}}$ .

### 3.3 Allyl Alcohol Selectivity

The initial selectivity of  $\text{TiO}_2/\text{Pt}/\text{SrTiO}_3$  for allyl alcohol (mean  $13.9\% \pm 0.3$ ) was higher than  $\text{Pt}/\text{SrTiO}_3$  ( $2.9\% \pm 0.5$ ) or  $\text{Al}_2\text{O}_3/\text{Pt}/\text{SrTiO}_3$  ( $3.2\% \pm 0.2$ ) (Table 2; Fig. 4). Initial selectivity for 1-propanol increased from  $\text{Pt}/\text{SrTiO}_3$  ( $1.3\% \pm 0.2$ ) to  $\text{Al}_2\text{O}_3/\text{Pt}/\text{SrTiO}_3$  ( $3.2\% \pm 0.3$ ) to  $\text{TiO}_2/\text{Pt}/\text{SrTiO}_3$  ( $6\% \pm 2$ ). No carbon monoxide was observed as a product during hydrogenation. The selectivity of acrolein hydrogenation was calculated from the mol% of the products (allyl alcohol, 1-propanol, propanal, Equation S8).

The increased allyl alcohol selectivity of  $\text{TiO}_2/\text{Pt}/\text{SrTiO}_3$  (13.9%) versus  $\text{Pt}/\text{SrTiO}_3$  (2.9%) is similar to the increased aldehyde hydrogenation selectivity observed in SMSI catalysts after HTR (e.g. an increase from 8 to 20% deuterated allyl alcohol selectivity with the HTR- $\text{Pt}/\text{TiO}_2$  SMSI catalyst) [22]. The more widely studied crotonaldehyde hydrogenation reaction has both a higher base selectivity and greater selectivity increase from SMSI (from 12.6 to 37.2% selectivity to crotyl alcohol after HTR); the base selectivity is increased as a result of steric hindrance by the methyl group destabilizing  $\text{C}=\text{C}$  bonding with Pt [15, 16,

**Table 2** Average acrolein hydrogenation selectivity at times initial and final

	Selectivity (%)					
	Allyl alcohol		1-Propanol		Propanal	
	Initial	Final	Initial	Final	Initial	Final
$\text{Pt}/\text{SrTiO}_3$	2.9(5)	3.5(5)	1.3(2)	1.1(1)	95.8(6)	95.4(6)
$\text{Al}_2\text{O}_3/\text{Pt}/\text{SrTiO}_3$	3.2(2)	4(1)	3.2(3)	3(1)	93.6(5)	93(1)
$\text{TiO}_2/\text{Pt}/\text{SrTiO}_3$	13.9(3)	6.5(8)	6(2)	3.5(7)	80(3)	90(1)

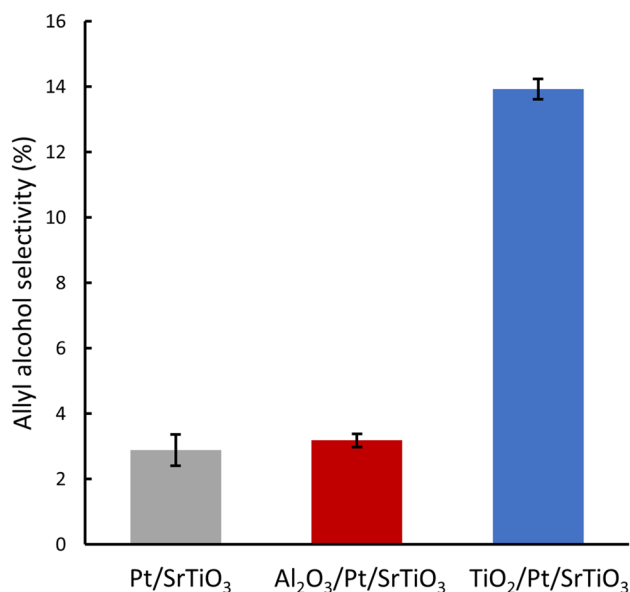


**Fig. 4** Initial allyl alcohol selectivity for Pt/SrTiO<sub>3</sub>, Al<sub>2</sub>O<sub>3</sub>/Pt/SrTiO<sub>3</sub>, and TiO<sub>2</sub>/Pt/SrTiO<sub>3</sub>

19]. Conversely, there is not a significant increase in allyl alcohol selectivity for Al<sub>2</sub>O<sub>3</sub>/Pt/SrTiO<sub>3</sub> (3.2%), even though there is partial coverage of the Pt<sub>np</sub> by the alumina overcoat. This indicates that there is no SMSI effect on selectivity for the alumina overcoat, as expected, because alumina is not predicted to form the interfacial sites necessary for SMSI catalysis [2].

The potential effects of structure sensitivity, an alternate suggestion for modifying the selectivity of catalysts, must also be considered [18, 79, 80]. In most examples of structure sensitivity, the size of the M<sub>np</sub> is modified to change selectivity [81]. Alternatively, structure sensitivity from modifying the shape of Pt<sub>np</sub> can change the selectivity of a reaction [34]. In addition, it may be possible to modify selectivity by blocking specific surface sites, i.e. with an overcoat [51]. The observed difference in initial selectivity for allyl alcohol between Pt/SrTiO<sub>3</sub> (2.9% ± 0.5) and Al<sub>2</sub>O<sub>3</sub>/Pt/SrTiO<sub>3</sub> (3.2% ± 0.2) from the available data (Fig. 4; Table 2) was not statistically significant. This is to be expected, as alumina ALD on Pt is not predicted to preferentially deposit on the low-coordination sites [76]. Instead, as seen in Fig. 1a, the alumina overcoat is observed primarily on the SrTiO<sub>3</sub> support, and covers Pt<sub>surf</sub> sites to the extent that the alumina film extends from the SrTiO<sub>3</sub> surface. The geometric, rather than preferential, coverage of the Pt<sub>np</sub> by the alumina overcoat is expected to have a small or negligible structure sensitivity effect on selectivity.

The structure-sensitive selectivity of acrolein hydrogenation to allyl alcohol, which increases with the size of the catalyst M<sub>np</sub>, can be approximated as the transition from a highly stepped single crystal to a perfectly flat single crystal

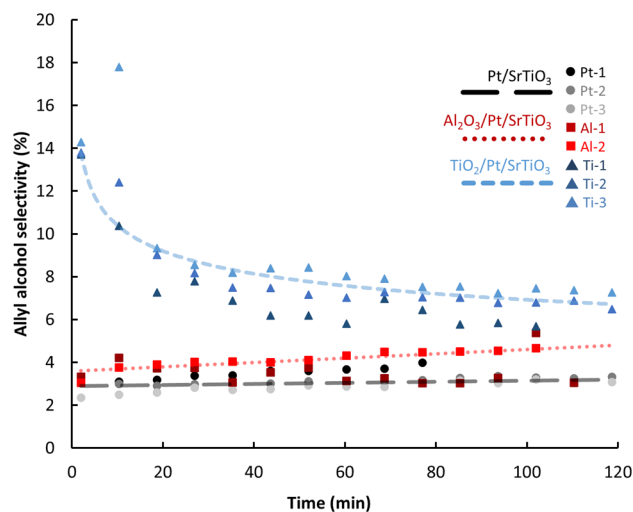


**Fig. 5** Allyl alcohol selectivity versus time. Selectivity decreased with time for TiO<sub>2</sub>/Pt/SrTiO<sub>3</sub>, and increased for the other two catalysts. The lines are drawn for illustrative purposes

[80]. Under this approximation, the selectivity of low-index facets (e.g. (111) or (100)) for a reaction can be considered theoretical maximums for unmodified nanoparticle catalysts (assuming no alloying, selective poisoning, etc.). The selectivity of Pt(111) and Pt(100) single crystals for the hydrogenation of crotonaldehyde to crotyl alcohol at 90 °C was 10%; selectivity for acrolein to allyl alcohol was not noted at that temperature on Pt single crystals, but was overall lower than the selectivity for crotyl alcohol [33]. A selectivity of 10% for the hydrogenation of crotonaldehyde to crotyl alcohol at 90 °C is then the theoretical maximum for Pt<sub>np</sub> catalysts. That the allyl alcohol selectivity of TiO<sub>2</sub>/Pt/SrTiO<sub>3</sub> is 13.9% at 100 °C, for a reaction which has a theoretical selectivity below 10% on Pt, indicates that the change in selectivity from the TiO<sub>2</sub> ALD overcoat is much greater than can be expected from structure sensitivity, and can be attributed to SMSI [18].

### 3.4 Allyl Alcohol Selectivity Deactivation

The selectivity of TiO<sub>2</sub>/Pt/SrTiO<sub>3</sub> for allyl alcohol decreased with time to 6.5% ± 0.8, as has previously been noted for SMSI catalysts [15], whereas the allyl alcohol selectivity of Pt/SrTiO<sub>3</sub> and Al<sub>2</sub>O<sub>3</sub>/Pt/SrTiO<sub>3</sub> increased with time (Table 2), as has previously been observed for Pt/SrTiO<sub>3</sub> [34]. At t = 120 min, allyl alcohol selectivity had stabilized; the selectivity of TiO<sub>2</sub>/Pt/SrTiO<sub>3</sub> for allyl alcohol remained higher than the other catalysts (Fig. 5).

The aldehyde hydrogenation selectivity of SMSI catalysts has been shown to be proportional to the concentration of interfacial sites (e.g. the TiO<sub>x</sub>-Pt interfacial sites of HTR-Pt/TiO<sub>2</sub> catalysts) [16, 21]. The rate of deactivation of the

interfacial sites depends on reaction conditions, which were not explored for the present system. Interfacial sites can be regenerated by migration from the oxide bulk [82], or hydrogen spillover from the  $M_{np}$  [83].

## 4 Conclusions

Here we have used ALD of titania and alumina on Pt/SrTiO<sub>3</sub> to re-create the overcoats observed in SMSI catalysts by a method other than HTR. We were curious as to whether the increased selectivity of SMSI catalysts for aldehyde hydrogenation would be observed for this alternative overcoat synthesis method. As expected, the selectivity of acrolein hydrogenation to allyl alcohol increased from 2.9 to 13.9% after the deposition of a titania overcoat, while the alumina-overcoat did not have a significant effect on selectivity (3.2% selectivity to allyl alcohol). While the average deposition thickness of the two overcoats was similar, their morphology was different. ALD alumina deposited primarily on SrTiO<sub>3</sub>, surrounding the perimeter of the Pt<sub>np</sub>, while ALD titania deposited on both Pt and SrTiO<sub>3</sub>. As a result, 95.7% of the Pt<sub>np</sub> surface was covered by a sub-nanometer film of titania. As a further consequence, nearly every exposed Pt atom should be at an interface with the titania overcoat, greatly increasing the probability of interfacial site formation versus an undecorated Pt<sub>np</sub>. The increased selectivity of the titania-coated Pt/SrTiO<sub>3</sub> for allyl alcohol, as well as the preferential growth of ALD titania on the Pt<sub>np</sub> are indicative of SMSI behavior resulting from interactions between the ALD titania overcoat and the Pt<sub>np</sub>, similar to the titania overcoats of HTR-Pt/TiO<sub>2</sub> catalysts. While the titania-overcoated Pt/SrTiO<sub>3</sub> examined here is not as selective for aldehyde hydrogenation as many examples of HTR-Pt/TiO<sub>2</sub>, it is likely that modification of the ALD overcoat thickness or pre-reduction conditions can increase selectivity, by increasing the concentration of interfacial defect sites.

These results suggest that ALD may be a new and versatile alternative to HTR for studying structure-properties relationships of SMSI catalysts. Future work would involve quantifying the number of interfacial sites and the degree of reduction of the titania overcoat while varying ALD overcoat thickness and pre-reduction conditions. Thin film deposition of SMSI-active oxides, such as titania, when deposited on non-reducible supports (e.g. alumina, silica, zeolites), may exhibit different properties than overcoats of the same oxides formed by HTR of a reducible support. For example, the non-reducible supports may pin defects in the overcoat, while in the case of HTR catalysts, there is migration of defects between the overcoat and the bulk of the support. An SMSI catalyst assembled as reducible oxide/ $M_{np}$ /non-reducible oxide may have a lower barrier to regenerating defect sites under operating conditions, as there would be

no migration of surface defects to the bulk, and the barrier to reduction tends to decrease with domain size. The support or an additional overcoat layer can also be used to introduce bifunctional catalysts (acids, bases, other metals) in combination with the SMSI catalyst. ALD of reducible oxide overcoats on supported metal catalysts opens a new range of opportunities for the study of SMSI catalysis.

**Acknowledgements** This material is based on work supported as part of the Institute for Atom-efficient Chemical Transformations (IACT), an Energy Frontiers Research Center funded by the U.S. Department of Energy, Office of Science, Office of Basic Energy Sciences. RMK and LAC acknowledge funding from Northwestern University Institute for Catalysis in Energy Processes (ICEP) on Grant No. DOE DE-FG02-03-ER15457. Electron microscopy was performed at the EPIC facility supported by the NU-MRSEC program (NSF DMR-1121262) and at the UIC Research Resources Center supported by the MRI-R<sup>2</sup> grant from the National Science Foundation (NSF DMR-0959470). The CleanCat Core facility acknowledges funding from the Department of Energy (DE-FG02-03-ER15457) used for the purchase of the Altamira AMI-200. Metal analysis was performed at the Northwestern University Quantitative Bio-element Imaging Center.

**Author Contributions** Electron microscopy was performed by LAC and AG. Atomic layer deposition of Pt and Al<sub>2</sub>O<sub>3</sub> was performed by CPC (Grace, formerly ANL) and JWE (ANL). Atomic layer deposition of TiO<sub>2</sub> was by KD (NU). This manuscript was written with contribution of all authors. All authors have given approval to the final version of the manuscript.

## Compliance with Ethical Standards

**Conflict of interest** The authors declare that they have no conflict of interest.

## References

1. Tauster SJ, Fung SC, Garten RL (1978) *J Am Chem Soc* 100:170–175
2. Tauster SJ, Fung SC (1978) *J Catal* 55:29–35
3. Huizinga T, Prins R (1981) *J Phys Chem* 85:2156–2158
4. Tauster SJ, Fung SC, Baker RT, Horsley JA (1981) *Science* 211:1121–1125
5. Tauster SJ (1987) *Acc Chem Res* 20:389–394
6. Haller GL, Resasco DE (1989) *Adv Catal* 36:173–235
7. Bernal S, Calvino JJ, Cauqui MA, Gatica JM, López Cartes C, Pérez Omil JA, Pintado JM (2003) *Catal Today* 77:385–406
8. Kliewer CE, Miseo S, Baumgartner JE, Stach EA, Zakharov D (2009) *Microsc Microanal* 15:1066–1067
9. Liu JJ (2011) *ChemCatChem* 3:934–948
10. Zhang S, Plessow PN, Willis JJ, Dai S, Xu M, Graham GW, Cargnello M, Abild-Pedersen F, Pan X (2016) *Nano Lett* 16:4528–4534
11. Ko EI, Hupp JM, Wagner NJ (1984) *J Catal* 86:315–327
12. O'Shea VA, Galvan MC, Prats AE, Campos-Martin JM, Fierro JL (2011) *Chem Commun (Camb)* 47:7131–7133
13. Bond GC (1983) *Platin Met Rev* 27:16–18
14. da Costa Faro A Jr, Kembal C (1995) *J Chem Soc Faraday Trans* 91:741–748
15. Vannice MA, Sen B (1989) *J Catal* 115:65–78
16. Vannice MA (1997) *Top Catal* 4:241–248

17. Vannice MA, Twu CC (1983) *J Catal* 82:213–222
18. Englisch M, Jentys A, Lercher JA (1997) *J Catal* 166:25–35
19. Dandekar A, Vannice MA (1999) *J Catal* 183:344–354
20. Yoshikata H, Iwasawa Y (1991) *J Catal* 125:227–242
21. Kennedy G, Baker LR, Somorjai GA (2014) *Angew Chem Int Ed Engl* 53:3405–3408
22. Yoshitake H, Iwasawa Y (1992) *J Chem Soc Faraday Trans* 88:503–510
23. Nelson RC, Baek B, Ruiz P, Goundie B, Brooks A, Wheeler MC, Frederick BG, Grabow LC, Austin RN (2015) *ACS Catal* 5:6509–6523
24. Serna P, Corma A (2015) *ACS Catal* 5:7114–7121
25. Corma A, Serna P, Concepción P, Juan Calvino J (2008) *J Am Chem Soc* 130:8748–8753
26. Kast P, Friedrich M, Teschner D, Girgsdies F, Lunkenbein T, Naumann d'Alnoncourt R, Behrens M, Schlögl R (2015) *Appl Catal A Gen* 502:8–17
27. Blankenburg KJ, Datye AK (1991) *J Catal* 128:186–197
28. Herrmann J-M (1989) *J Catal* 118:43–52
29. Duprez D, Miloudi A (1982) In: Imelik B, Coudurier G, Praliaud H, Meriaudeau P, Gallezot P, Martin GA, Vadrine JC, BT—Studies in Surface Science and Catalysis CN (eds) Metal-Support and Metal-Additive Effects in Catalysis Proceedings of an International Symposium organized by the Institut de Recherches sur la Catalyse—CNRS—Villeurbanne and sponsored by the Centre National de la Recherche Scientifique. Elsevier, New York, pp 179–184
30. Ajayan PM, Marks LD (1989) *Nature* 338:139–141
31. Liu W, Jiang Y, Dostert KH, O'Brien CP, Riedel W, Savara A, Schauermaann S, Tkatchenko A (2017) *Sci Adv* 3:1–8
32. Gallezot P, Richard D (1998) *Catal Rev Sci Eng* 40:81–126
33. Kliewer CJ, Bieri M, Somorjai GA (2009) *J Am Chem Soc* 131:9958–9966
34. Enterkin JA, Kennedy RM, Lu J, Elam JW, Cook RE, Marks LD, Stair PC, Marshall CL, Poepelmeier KR (2013) *Top Catal* 56:1829–1834
35. Engelhardt C, Kennedy RM, Enterkin J, Poepelmeier K, Ellis D, Marshall C, Stair P (2018) *ChemCatChem* 10:632–641
36. Azadi P, Carrasquillo-Flores R, Pagán-Torres YJ, Gürbüz EI, Farnood R, Dumesic JA (2012) *Green Chem* 14:1573
37. Mariscal R, Maireles-Torres P, Ojeda M, Sádaba I, López Granados M (2016) *Energy Environ Sci* 9:1144–1189
38. Krahling L, Krey J, Jakobson G, Grolig J, Miksche L (2000) Ullmann's encyclopedia of industrial chemistry. Wiley, Hoboken
39. Singh UK, Vannice MA (2001) *Appl Catal A Gen* 213:1–24
40. Moberg DR, Thibodeau TJ, Amar FG, Frederick BG (2010) *J Phys Chem C* 114:13782–13795
41. Dong Y, Zaera F (2018) *J Phys Chem Lett* 9:1301–1306
42. de Jesús JC, Zaera F (1999) *Surf Sci* 430:99–115
43. Lu J, Elam JW, Stair PC (2016) *Surf Sci Rep* 71:410–472
44. Puurunen RL (2005) *J Appl Phys* 97:121301
45. Knapas K, Ritala M (2013) *Crit Rev Solid State Mater Sci* 38:167–202
46. George SM (2010) *Chem Rev* 110:111–131
47. Stair PC (2008) *J Chem Phys* 128:182507
48. Alba-Rubio AC, O'Neill BJ, Shi F, Akatay C, Canlas C, Li T, Winans R, Elam JW, Stach EA, Voyles PM, Dumesic JA (2014) *ACS Catal* 4:1554–1557
49. Lu J, Fu B, Kung MC, Xiao G, Elam JW, Kung HH, Stair PC (2012) *Science* 335:1205–1208
50. Canlas CP, Lu J, Ray NA, Grosso-Giordano NA, Lee S, Elam JW, Winans RE, Van Duyne RP, Stair PC, Notestein JM (2012) *Nat Chem* 4:1030–1036
51. O'Neill B, Jackson DHK, Lee J, Canlas C, Stair PC, Marshall CL, Elam JW, Kuech TF, Dumesic JA, Huber GW (2015) *ACS Catal* 15:1804
52. Boudart M (2000) *Top Catal* 13:147–149
53. Lin Y, Wen J, Hu L, Kennedy RM, Stair PC, Poepelmeier KR, Marks LD (2013) *Phys Rev Lett* 111:156101
54. Crosby LA, Kennedy RM, Chen B-R, Wen J, Poepelmeier KR, Bedzyk MJ, Marks LD (2016) *Nanoscale* 8:16606–16611
55. Crosby LA, Chen B-R, Kennedy RM, Wen J, Poepelmeier KR, Bedzyk MJ, Marks LD (2018) *Chem Mater* 30:841–846
56. Crosby L, Enterkin J, Rabuffetti F, Poepelmeier KR, Marks L (2015) *Surf Sci* 632:L22–L25
57. Enterkin JA, Poepelmeier KR, Marks LD (2011) *Nano Lett* 11:993–997
58. Enterkin JA, Setthapun W, Elam JW, Christensen ST, Rabuffetti FA, Marks LD, Stair PC, Poepelmeier KR, Marshall CL (2011) *ACS Catal* 1:629–635
59. Christensen ST, Elam JW, Rabuffetti FA, Ma Q, Weigand SJ, Lee B, Seifert S, Stair PC, Poepelmeier KR, Hersam MC, Bedzyk MJ (2009) *Small* 5:750–757
60. Setthapun W, Williams WD, Kim SM, Feng H, Elam JW, Rabuffetti FA, Poepelmeier KR, Stair PC, Stach EA, Ribeiro FH, Miller JT, Marshall CL (2010) *J Phys Chem C* 114:9758–9771
61. Lin Y, McCarthy JA, Poepelmeier KR, Marks LD (2015) Applications of electron microscopy in heterogeneous catalysis. Elsevier, New York
62. Yang X, Mueannern Y, Baker QA, Baker LR (2016) *Catal Sci Technol* 6:6824–6835
63. Wang C, Wang H, Yao Q, Yan H, Li J, Lu J (2016) *J Phys Chem C* 120:478–486
64. Yao Q, Wang C, Wang H, Yan H, Lu J (2016) *J Phys Chem C* 120:9174–9183
65. Bai Y, Wang C, Zhou X, Lu J, Xiong Y (2016) *Prog Nat Sci Mater Int* 26:289–294
66. Rabuffetti FA, Kim H-S, Enterkin JA, Wang Y, Lanier CH, Marks LD, Poepelmeier KR, Stair PC (2008) *Chem Mater* 20:5628–5635
67. Lu J, Stair PC (2010) *Langmuir* 26:16486–16495
68. Ray NA, Van Duyne RP, Stair PC (2012) *J Phys Chem C* 116:7748–7756
69. Lu J, Kosuda KM, Van Duyne RP, Stair PC (2009) *J Phys Chem C* 113:12412–12418
70. Brunauer S, Emmett PH, Teller E (1938) *J Am Chem Soc* 60:309–319
71. Freil J (1972) *J Catal* 160:149–160
72. Li T, Karwal S, Aoun B, Zhao H, Ren Y, Canlas CP, Elam JW, Winans RE (2016) *Chem Mater* 28:7082–7087
73. Miikkulainen V, Leskelä M, Ritala M, Puurunen RL (2013) *J Appl Phys* 113:021301
74. Rase HF (1990) Fixed-bed reactor design and diagnostics: gas-phase reactions. Butterworths, London
75. Lu J, Liu B, Greeley JP, Feng Z, Libera JA, Lei Y, Bedzyk MJ, Stair PC, Elam JW (2012) *Chem Mater* 24:2047–2055
76. Lu J, Liu B, Guisinger NP, Stair PC, Greeley JP, Elam JW (2014) *Chem Mater* 26:6752–6761
77. Ono LK, Yuan B, Heinrich H, Cuenya BR (2010) *J Phys Chem C* 114:22119–22133
78. Zhang Z, Li L, Yang JC (2013) *J Phys Chem C* 117:21407–21412
79. Somorjai GA, Carrarza J (1986) *Ind Eng Chem Fundam* 25:63–69
80. Che M, Bennett CO (1989) *Adv Catal* 36:55–172
81. Wei H, Gomez C, Liu J, Guo N, Wu T, Lobo-Lapidus R, Marshall CL, Miller JT, Meyer RJ (2013) *J Catal* 298:18–26
82. Weerachawanasak P, Praserttham P, Arai M, Panpranot J (2008) *J Mol Catal A* 279:133–139
83. Prins R (2012) *Chem Rev* 112:2714–2738

## Affiliations

Robert M. Kennedy<sup>1</sup>  · Lawrence A. Crosby<sup>2</sup>  · Kunlun Ding<sup>3</sup>  · Christian P. Canlas<sup>4</sup>  · Ahmet Gulec<sup>2</sup>  ·  
Laurence D. Marks<sup>2</sup> · Jeffrey W. Elam<sup>4</sup>  · Christopher L. Marshall<sup>5</sup>  · Kenneth R. Poepelmeier<sup>1,5</sup>  ·  
Peter C. Stair<sup>1,5</sup> 

Robert M. Kennedy  
rmk@u.northwestern.edu

Lawrence A. Crosby  
crosbyla@u.northwestern.edu

Kunlun Ding  
kunlunding@lsu.edu

Christian P. Canlas  
Christian.Canlas@grace.com

Ahmet Gulec  
ahmet.gulec@northwestern.edu

Laurence D. Marks  
l-marks@northwestern.edu

Jeffrey W. Elam  
jelam@anl.gov

Christopher L. Marshall  
Marshall@anl.gov

Kenneth R. Poepelmeier  
krp@northwestern.edu

<sup>1</sup> Department of Chemistry, Northwestern University,  
Evanston, IL 60208, USA

<sup>2</sup> Department of Materials Science and Engineering,  
Northwestern University, Evanston, IL 60208, USA

<sup>3</sup> Chemical Engineering, Louisiana State University,  
Baton Rouge, LA 70803, USA

<sup>4</sup> Energy Systems Division, Argonne National Laboratory,  
Lemont, IL 60439, USA

<sup>5</sup> Chemical Sciences and Engineering Division, Argonne  
National Laboratory, Lemont, IL 60439, USA